Influence of electrode Fermi energy on interband tunneling

A. Nogaret,* D. K. Maude, and J. C. Portal
Laboratoire de Physique des Solides, Institut National des Sciences Appliquées, 31077 Toulouse Cedex, France and Service National des Champs Intenses, Centre National de la Recherche Scientifique, 38042 Grenoble Cedex, France

M. A. Maldonado, K. P. Martin, R. E. Carnahan, and R. J. Higgins
School of Electrical Engineering and Microelectronics Research Center, Georgia Institute of Technology, Atlanta, Georgia 30332-0269

H. Lee and A. Y. Cho
AT&T Bell Laboratories, Murray Hill, New Jersey 07974
(Received 17 June 1994; revised manuscript received 29 November 1994)

The choice of the Fermi energy in the electrodes of a GaSb/AlSb/InAs/AlSb/GaSb type-II heterostructure has deep consequences on the physics of interband tunneling. We show that tunneling between electron and hole bands will result in three different current-voltage characteristics depending on the Fermi energy in the electrodes of the device. When electrode doping is high, the device characteristics exhibit a current shoulder at low bias followed by a current peak. Magnetotunneling experiments reveal additional current satellites: one emerging from the shoulder and another one emerging from the peak. The shift in the voltage position of these two features and that of the peak current is opposite when the magnetic field increases. This splitting is evidence of a hybridization gap due to $\mathbf{k}\cdot\mathbf{p}$ coupling between the electron band in InAs and the hole bands in GaSb.

INTRODUCTION

In type-I resonant tunneling structures, the composition and size parameters of the double barrier and quantum well that form the active region determine most features of technological interest, such as the peak to valley current ratio, the dwell time, and the peak current.[1,2] The doping level in the electrodes has a comparatively minor influence on the current-voltage characteristics of such systems: increasingly large electrode Fermi energies widen the peaks of resonance.[3] The doping level in the vicinity of the emitter barrier also controls the dimensionality of the injected carriers and the scattering potential they experience, due to screened impurities.[4] Type-II heterostructures stimulated an interest in tunneling as it was realized that negative differential resistances could also arise from the peculiar band alignment of the GaSb/AlSb/InAs material system. The valence band in GaSb lies 150 meV (Ref. 5) higher than the conduction band in InAs. Negative differential resistance originates from the closure of this energy window when an external bias makes the InAs and GaSb band gaps overlap. Several devices based on this principle have been implemented often with greatly improved performances over type-I double-barrier structures.[6–9] Mendez *et al.* were the first, to our knowledge, to relate magnetotunnel phenomena to interband tunneling[10] and to describe the consequences of in-plane momentum conservation in type-II heterostructures.[11]

In the first part of this paper, we show that depending on the value of the electrode Fermi energy, a type-II tunneling structure can exhibit three different types of I-V characteristics (whereas only one is expected in conventional double-barrier structures). A simple free particle model is implemented which provides an accurate description of our experiment. In the second part of this paper, a magnetic field applied perpendicular to the layers reveals satellite features in the I-V's, which move to higher bias voltage with increasing magnetic field. This observation can be explained by an improved model in which electrons and holes are not free particles, but instead are coupled via the $\mathbf{k}\cdot\mathbf{p}$ interaction.

TUNNELING BETWEEN PARABOLIC BANDS

A conceptually simple picture of tunneling is to consider electrons and holes as free particles (with parabolic dispersion curves) that tunnel in the absence of scattering with the conservation of both energy and in-plane momentum.[12] Hence, the resonant current density ($J_{\rm res}$) is simply proportional to the number of tunneling channels [$N_{\rm 2D}(V_b)$] resulting from the overlapping between the resonant subband and the electron/hole distributions in the electrodes:[13]

$$J_{\rm res}=eN_{\rm 2D}(V_b)\frac{\Gamma}{\hbar}T_{\rm res}\ , \tag{1}$$

where $T_{\rm res}$ is the transmission probability at resonance, V_b is the bias voltage, Γ is the resonance energy width, e and $\hbar$ are fundamental constants. Our purpose, in this section, is to discuss the modifications that a gradual increase in the electrode Fermi energy would induce in the I-V characteristic of a GaSb/AlSb/InAs/AlSb/GaSb tunneling structure [Fig. 1(a)]. The three-dimensional (3D) hole distribution in the collector acts as an energy and momentum spectrometer with both energy (the hole Fermi energy) and in-plane momentum (the hole Fermi momentum) linewidths. Doping the electrodes can tune

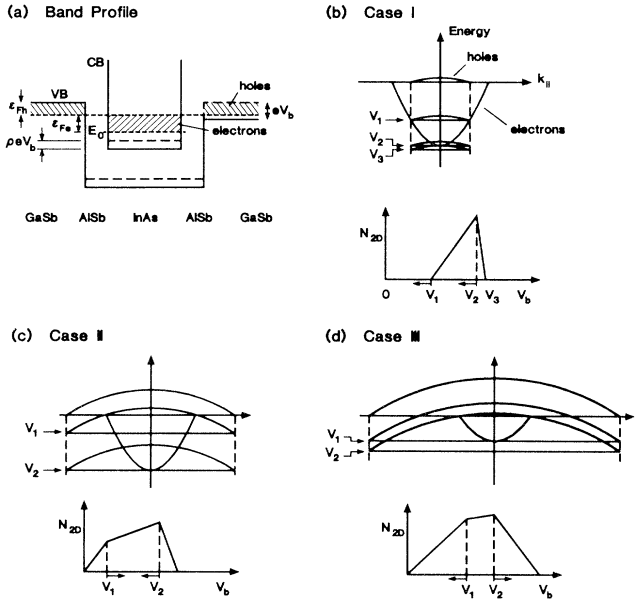

FIG. 1. (a) Schematic flat band profile of the active region of our sample with (full lines) and without (dashed lines) an applied bias V_b. The parameters ρ and ε_{Fe} used to fit the voltage position of the experimental features are also shown. ε_{Fh} is the hole Fermi energy set by the electrode doping level and E_0 labels the resonant state. (b), (c), (d) show the different stages of the electron (well) and hole (collector) distribution overlap that produce the turning points at $V_b=V_1$, V_2 and V_3 in the $N_{2D}(V_b)$ traces. (b), (c), (d), respectively, refer to the low-, intermediate-, and high-doping levels as discussed in the text. For each case, the arrows in the $N_{2D}(V_b)$ traces indicate the expected shift of the features when the hole Fermi energy increases.

both parameters with respect to the maximum energy and in-plane momentum of the electrons traversing the structure at resonance. Hence, geometrical construction for different overlaps of the 2D electron distribution in the well (i.e., the 2D subband in the well populated up to the emitter Fermi level) with the 3D hole distribution in the collector [Fig. 1(a)] leads to $N_{2D}(V_b)$. Henceforth, these two distributions will be referred to as the electron and hole distribution, respectively. Starting from intrinsic electrodes and increasing their doping level, three different types of I-V characteristics are successively expected [Figs. 1(b), 1(c), 1(d)].

In an intrinsic and ideally symmetric structure at equilibrium, *case I*, holes equally distribute among each electrode with a density half that of the electrons in the well. The condition of momentum conservation precludes all electrons with an in-plane momentum larger than the hole Fermi momentum from tunneling into the collector [Fig. 1(b)], therefore the I-V curve shows a current onset at $V_b=V_1$.[11] The peak current at $V_b=V_2$ occurs when the collector Fermi level aligns with the bottom of the resonant subband [Fig. 1(b)]. For this low-doping regime,

$$eV_1=\frac{m_e^*\varepsilon_{Fe}-m_h^*\varepsilon_{Fh}}{(1-\rho)m_e^*},\quad eV_2=\frac{\varepsilon_{Fe}}{1-\rho},\quad eV_3=\frac{\varepsilon_{Fh}+\varepsilon_{Fe}}{1-\rho}, \tag{2}$$

m_h^* and m_e^* are the density-of-states effective masses of the hole and electron distributions, and ρeV_b $(0<\rho<1)$ is the potential-energy drop from the emitter electrode to the well [Fig. 1(a)]. ε_{Fe} is the Fermi energy of the electrons at zero bias and ε_{Fh} is the Fermi energy of the holes.

When the hole Fermi wave vector becomes larger than the electron Fermi wave vector, *case II*, the condition of in-plane momentum conservation no longer inhibits electrons with the highest energy from tunneling into the collector and the onset voltage disappears. Instead, a current shoulder[14] emerges at $V_b=V_1$, when the overlap of the hole distribution by the electron distribution is completed [Fig. 1(c)]. At higher bias voltages, $V_b>V_1$, the current increases more slowly as fewer tunneling channels can be added through the hole distribution. For this intermediate electrode doping regime, we obtain

$$eV_1=\frac{m_h^*\varepsilon_{Fh}-m_e^*\varepsilon_{Fe}}{m_h^*+\rho m_e^*},\quad eV_2=\frac{\varepsilon_{Fe}}{1-\rho}. \tag{3}$$

The third type of I-V curve, *case III*, is achieved when the hole Fermi energy exceeds the electron Fermi energy at the peak current. V_1 and V_2 now define the boundaries of a bias voltage range in which the electron distribution remains completely overlapped by the hole distribution [Fig. 1(d)]. For this heavy doping regime,

$$eV_1=\frac{\varepsilon_{Fe}}{1-\rho},\quad eV_2=\frac{m_h^*\varepsilon_{Fh}-m_e^*\varepsilon_{Fe}}{m_h^*+\rho m_e^*}. \tag{4}$$

Reference 11 has particularly demonstrated the relevance of this simple description by investigating the low-doping regime. In this paper, we will report on results for a similar structure with a higher-doping level in the contacts, in order to illustrate one of the two other cases. Our structures were grown by molecular-beam epitaxy on a p^+ GaAs substrate, according to the following sequence: (i) 1.5 μm $p^+=2\times10^{18}$ cm^{-3} GaSb buffer; (ii) 5-nm-undoped GaSb spacer; (iii) 4-nm-undoped AlSb barrier; (iv) 16-nm-undoped InAs well; (v) 4-nm-undoped AlSb barrier; (vi) 5-nm-undoped GaSb spacer; (vii) 1.5-μm $p^+=2\times10^{18}$ cm^{-3} GaSb cap layer. The devices presented in this study have a 15×15 μm^2 mesa area.

The I-V curves measured at 4.2 K (Fig. 2) effectively show a shoulder at $V_s=54$ mV and a peak current at $V_p=145$ mV. For bias voltages below 60 mV, periodic magneto-oscillations in the current are observed and analyzed using a second derivative filter (inset Fig. 2). We ascribe the origin of these oscillations to Landau levels formed in the electrodes since a frequency related to Landau levels in the well would depend on bias voltage. Such dependence is not observed in the 10–60-mV bias range. Using the light-hole effective mass $m_{lh}^*=0.05m_o$,[15] we can estimate $\varepsilon_{Fh}=57\pm11$ meV, which is in agreement within a factor 2 with the nominal dopant density in the electrodes.

By substituting the experimental values (V_s,V_p) to (V_1,V_2) in Eqs. (3) and (4), one can solve a set of two equations in which there are two unknowns ρ and ε_{Fe}. Using standard material parameters[15] and the experimen-

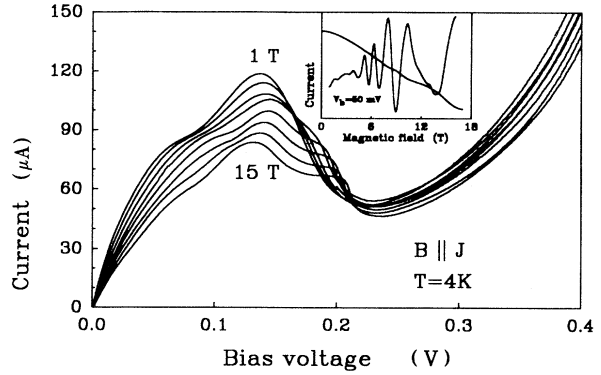

FIG. 2. Experimental current-voltage characteristics at magnetic fields from 1 to 15 T in 2 T steps. The presence of a current shoulder, $V_s = 54$ mV, and a peak current, $V_p = 145$ mV, at vanishing magnetic fields is the signature of device with an intermediate-doping level (see text). Inset exhibits a current-magnetic-field curve at $V_b = 50$ mV. Its second derivative shows oscillations periodic in $1/B$ ascribed to Landau levels formed in the electrodes.

tal value for ε_{Fh}, the solutions assuming case II are $\rho = 0.64$ meV and $\varepsilon_{Fe} = 52$ meV, whereas those assuming case III are physically meaningless. In order to check the accuracy of this method, we reobtain ε_{Fe} from numerical calculations. The structure band profile [Fig. 3(b)] is calculated with a Poisson solver[16] in which ε_{Fh} and the accepted band offsets for this material system[17] are included as parameters. The quantum-mechanical transmission spectrum is then computed [Fig. 3(a)] within a two-band formalism.[18] Figure 3(a) shows two transmission peaks related to the ground (E_0) and first excited state (E_1) in the InAs well. Drawing E_0 and E_1 on the band profile [Fig. 3(b)] gives the theoretical energy spacings in the active region and in particular $\varepsilon_{Fe} = 58$ meV.

We, thus, conclude that our devices verify the intermediate doping regime. The parabolic band model can explain all of the observed features in the current-voltage

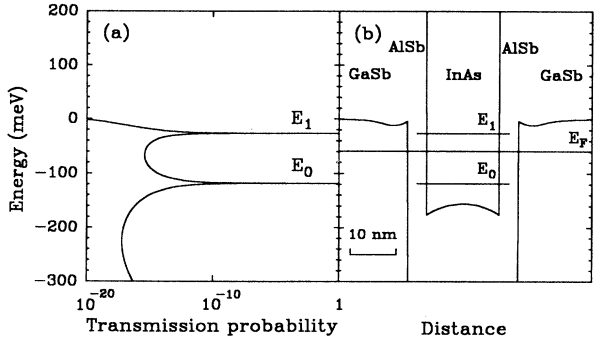

FIG. 3. The transmission spectrum (a) of the calculated potential profile (b) shows two bound levels E_0 and E_1 in the interband tunneling energy width. Only the ground state E_0 is resonant. Energy separations of interest are shown in the active region (b), the energy reference is taken at the valence-band edge in the flat potential region of the GaSb electrodes.

characteristics. Moreover, we have devised a simple and accurate method to obtain fundamental structural parameters from the voltage position of these features.

MAGNETIC-FIELD STUDY

The application of a magnetic field (B) perpendicular to the layers strongly affects the I-V curves in the region of the resonance (Fig. 2). To follow this evolution, we plot the bias position of the features as a function of the magnetic field (Fig. 4). The shoulder and peak current can be traced up to magnetic fields of 16 T. The voltage position of the peak slightly increases until 5 T, then decreases almost linearly up to 16 T. The shoulder has a complicated behavior in the range of intermediate magnetic fields, but it is still observed above 13 T at about the same position as at zero-magnetic field. Emerging from both the shoulder and peak are two marked satellites that continuously move towards higher biases with increasing magnetic field.[19]

High magnetic fields quantize the in-plane motion of electrons and holes into Landau levels. Their energy dependence as a function of B determines the evolution of the I-V curves. Multiband calculations performed for InAs/GaSb superlattices[20] show strongly nonlinear electron and hole Landau levels that anticross, because conduction and valence bands couple through $\mathbf{k}\cdot\mathbf{p}$ interaction terms.[21] For the sake of simplicity and without the loss of any essential physics, we model the band structure of the well-collector heterojunction as one hole band in GaSb and one-electron band in InAs both parabolic and coupled through a $\mathbf{k}\cdot\mathbf{p}$ term proportional to the Kane matrix element P. Following,[20] the effective Hamiltonian is written:

$$H(k_{\parallel}) = \begin{bmatrix} -\alpha k_{\parallel}^2 & P(k_x + ik_y) \\ P(k_x - ik_y) & E_0 + \beta k_{\parallel}^2 \end{bmatrix}, \tag{5}$$

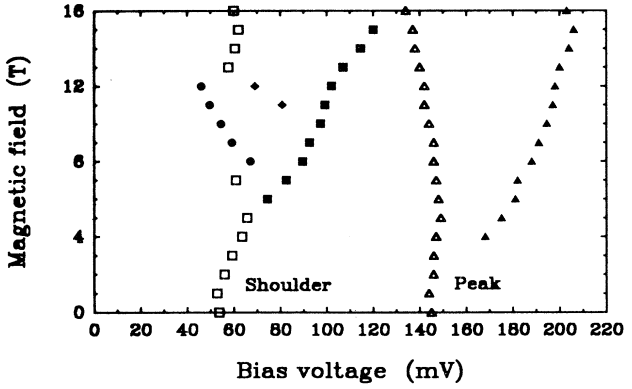

FIG. 4. Bias voltage position of the current features as a function of magnetic field. Note the shift of the peak (open triangles) to lower biases, the invariance of the shoulder (open squares), the shift of the peak (filled triangles), and shoulder (filled squares) satellites to higher biases with increasing magnetic fields. The filled circles and filled diamonds indicate weaker current features, whose physical origin is not clearly identified.

where $k_{\parallel}=(k_x,k_y)$ is the in-plane wave vector. The eigenvalues of the Hamiltonian [Eq. (5)] form the energy spectrum plotted as a function of the magnetic field in Fig. 5(a). Neglecting the off-diagonal terms in Eq. (5) ($P=0$), the magnetic confinement linearly shifts InAs electron and GaSb hole Landau levels in opposite directions along the energy axis [dashed lines, Fig. 5(a)]. Their crossing simply results from the effective-mass sign reversal from conduction to valence band. When off-diagonal terms are considered in Eq. (5), Landau levels show a mixed electron-hole character [full lines, Fig. 5(a)]. The nth hole Landau levels anticross with the $(n-1)$th electron Landau levels giving rise to an hybridization gap and only the $n=0$ level conserves a pure hole character.

The parabolic band approximation ($P=0$) introduced in the first section still provides a good understanding of the behavior of the peak and shoulder in the presence of a magnetic field. The voltage position of the peak linearly shifts to a lower bias voltage ($dV_p/dB=-1.4$ mV/T) to compensate for the reduction in the electron-hole overlap, essentially due to the elevation of the ground Landau level in the well. The shoulder appears at a bias voltage $V_b=V_s$ for which electron and hole Landau levels intersect at the electron Fermi level.[22] Because these intersections all happen at the same energy whatever the Landau index [Fig. 5(a)], the bias voltage required to align them with the electron Fermi level should be independent of B. This is experimentally verified since V_s is invariant with B (Fig. 4). However, the parabolic band model cannot account for the shift to higher bias voltages of the satellites of the peak and of the shoulder when B increases. This is because the intersection of electron and hole Landau levels of index n [Fig. 5(a)] define a magnetic field B_n above which tunneling is forbidden by the conservation of energy. Consequently, the I-B curves would exhibit magneto-oscillations peaked at $B=B_n$, followed by a zero conduction regime when $B>B_0$. This zero conduction regime is not observed even at our maximum magnetic-field value for $V_2<V_b<V_3$, when the electron-hole overlap tends to zero.

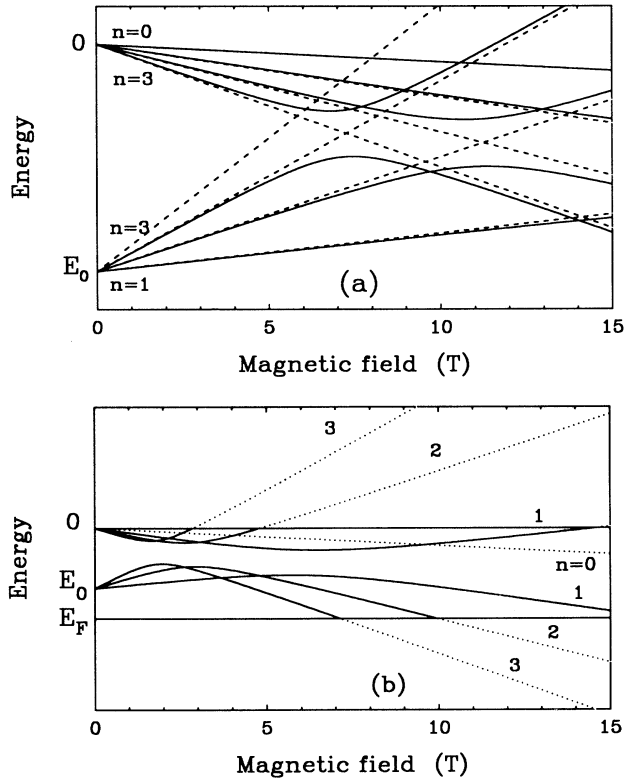

FIG. 5. (a) Calculated energy spectrum of the well-collector heterojunction as a function of magnetic field and at $V_b=0$. Without $\mathbf{k}\cdot\mathbf{p}$ interaction terms electron and hole Landau levels gain in opposite directions and cross (dashed lines). In presence of $\mathbf{k}\cdot\mathbf{p}$ coupling, Landau levels anticross, except for the $n=0$ branch, which keeps a pure hole character and does not contribute to tunneling (full lines and indexation). (b) Same energy spectrum calculated for $V_2<V_b<V_3$: the hole distribution (delimited by the horizontal lines at 0 and E_F) now completely overlaps the hybridization gap. All hybrid states (full lines) participate to the conduction, whereas electronlike holelike branches (dotted lines) are nonconducting. In both plots, the zero energy is at the valence-band edge of the collector electrode.

The $\mathbf{k}\cdot\mathbf{p}$ coupling relaxes the selection rules for tunneling from well to collector.[23] The new eigenstates of the system have strongly delocalized wave functions in the anticrossing regions, thus the maximum tunneling probability occurs in conditions similar to those expected if the levels in InAs and GaSb were crossing. Further away from each anticrossing, electronlike (hole-like) branches involve states which still have a probability in the hole (electron) band [Fig. 5(a)]. Thus, the hybridization of Landau levels still permits tunneling in a magnetic field range ($B>B_n$) forbidden in the parabolic band picture. We, therefore, make the assumption that the hybrid states give rise to an extra current whenever the selection rules limit the amount of tunneling channels, that is after the shoulder and the peak. From Eq. (5), the hybridization gap ΔE_n at the anticrossing of Landau level n can be expressed as

$$\Delta E_n(V_b)=\left[\frac{8nP^2(1-\rho)(eV_3-eV_b)}{2n(\alpha+\beta)+(\alpha-\beta)}\right]^{1/2},\quad n>0\ . \tag{6}$$

ΔE_n decreases with increasing V_b and also decreases with increasing n because in bulk materials, the curvature of the electron band, β, is always greater than that of any hole band, α. The satellites behavior (related to either the peak or the shoulder) in Fig. 4 may derive from the two following competing mechanisms. An increase in B increases the proportion of tunneling carriers in low index Landau levels [Fig. 5(b)], and the hybridization gap averaged over all carriers $\langle\Delta E_n\rangle$ thus increases [Eq. (6)]. Consequently, the average transfer rate $1/\tau=\langle\Delta E_n\rangle/\hbar$ between electrons and holes states increases entailing a B induced increase in the current. However, an increase in bias voltage V_b decreases ΔE_n [Eq. (6)], and thus diminishes the hybrid character of each branch [Fig. 5(b)]. By the same argument, the transfer rate between electron and hole states is reduced entailing a V_b induced decrease of the tunnel current. Equation (6) suggests that the satellites cannot move in the valley region beyond $V_b=V_3$,

because electron and hole bands completely decouple [$\Delta E_n(V_3)=0$] as their energy overlap ceases. In summary, the limitation of the number of tunneling channels by the selection rules leads to the observation of a shoulder and a peak current. We have assumed the existence of hybrid electron-hole states to explain the satellite features in the *I-V*'s and shown that the intrinsic properties of the hybridization gap permit us to understand the observed magnetic-field behavior.

We terminate this section by stressing the necessity for having large Fermi energy in order to evidence electron-hole coupling. The hybrid states will carry a current as long as their occupancy probability remains low in the collector, i.e., when the hole Fermi energy is large enough to overlap with the hybridization gap [Fig. 5(b)]. On the contrary, when the hole Fermi energy is small, case I, the hybridization gap lies below the hole Fermi level. In that case, tunneling only involves the weakly mixed electron states [Fig. 5(a)] above the hybridization gap and, therefore, no satellite should be expected.

CONCLUSION

In this paper, we have shown that a free particle model applied to interband tunneling predicts three types of current-voltage characteristics in samples with different carrier concentration in the electrodes. Two of them have been evidenced experimentally.

Investigations under magnetic-field confirm the physical origin of the peak and the shoulder in the current-voltage curves, but the data also show striking discrepancies from the picture where tunneling occurs between parabolic electron and hole bands. The splitting of the peak and shoulder can be explained simply by considering the existence of a hybridization gap, due to $\mathbf{k}\cdot\mathbf{p}$ coupling between electron and hole bands. These deviations from the parabolic band model should be observed whenever the hole collector Fermi energy is wide enough to overlap with the hybridization gap.

ACKNOWLEDGMENTS

We acknowledge financial support from the Conseil Régional Midi Pyrénées, the EEC, the CNRS/GDR, the CNRS/NSF, NATO institutions and France Auto Citroen Toulouse Montaudran. Support also came from NSF under Grant Nos. ECS-8922512 and INT-8815314.

*Also at the Georgia Institute of Technology, Atlanta, GA 30332-0269.

[1]T. Weil and B. Vinter, Appl. Phys. Lett. **50**, 1281 (1987).

[2]B. Ricco and M. Ya. Azbel, Phys. Rev. B **29**, 1970 (1984).

[3]E. E. Mendez, L. Esaki, and W. I. Wang, Phys. Rev. B **33**, 2893 (1986).

[4]A. Sugimura, Phys. Rev. B **47**, 9676 (1993).

[5]G. J. Gualtieri, G. P. Schwartz, R. G. Nuzzo, and W. A. Sunder, J. Appl. Phys. **61**, 5337 (1987).

[6]L. F. Luo, R. Beresford, and W. I. Wang, Appl. Phys. Lett. **55**, 2023 (1989).

[7]K. F. Longenbach, L. F. Luo, and W. I. Wang, Appl. Phys. Lett. **57**, 1554 (1990).

[8]J. R. Söderström, D. H. Chow, and T. C. McGill, Appl. Phys. Lett. **55**, 1094 (1989).

[9]L. Yang, J. F. Chen, and A. Y. Cho, J. Appl. Phys. **68**, 2997 (1990).

[10]E. E. Mendez, H. Ohno, L. Esaki, and W. I. Wang, Phys. Rev. B **43**, 5196 (1991).

[11]E. E. Mendez, J. Nocera, and W. I. Wang, Phys. Rev. B **45**, 3910 (1992).

[12]S. Luryi, Appl. Phys. Lett. **47**, 490 (1985).

[13]H. Ohno, E. E. Mendez, and W. I. Wang, Appl. Phys. Lett. **56**, 1793 (1990).

[14]A. Nogaret, M. A. Maldonado, R. E. Carnahan, K. P. Martin, R. J. Higgins, F. Aristone, D. K. Maude, J. C. Portal, J. F. Chen, and A. Y. Cho, Phys. Rev. B **47**, 13 872 (1993).

[15]$m_e^*=0.023m_0$, $m_h^*=0.31m_0$, where the hole density-of-state effective mass $m_h^*=(m_{hh}^{*3/2}+m_{lh}^{*3/2})^{2/3}$ is deduced from the heavy-hole $m_{hh}^*=0.30m_0$ and light-hole $m_{lh}^*=0.05m_0$ effective masses. m_e^*, m_{hh}^*, m_{lh}^* are taken from the tables of *Intrinsic Properties of Group IV Elements and III-V, II-VI and I-VII Compounds,* edited by O. Madelung, Landolt-Börnstein, New Series, Group III, Vol. 22, Pt. a (Springer Verlag, Berlin, 1982).

[16]M. S. Lundstrom and R. J. Schuelke, IEEE Trans. Electron Devices **9**, 1151 (1983).

[17]$E_{GAP}(InAs)=0.418$ eV, $E_{GAP}(AlSb)=1.696$ eV, $E_{GAP}=0.811$ eV; $\Delta E_{CB}(AlSb/InAs)=1.366$ eV, $\Delta E_{VB}(AlSb/InAs)=0.088$ eV; $\Delta E_{CB}(GaSb/InAs)=0.961$ eV, $\Delta E_{VB}(GaSb/InAs)=0.568$ eV.

[18]G. Bastard, J. A. Brum, and R. Ferreira, in *Solid State Physics: Advances in Research and Applications,* edited by H. Ehrenreich and D. Turnbull (Academic, New York, 1991), pp. 229–415.

[19]The observation of the peak satellite is allowed because the *I-V* characteristic is stable in the NDR region.

[20]A. Fasolino and M. Altarelli, Surf. Sci. **142**, 322 (1984).

[21]M. Altarelli, Phys. Rev. B **28**, 842 (1983).

[22]States in the collector have a zero longitudinal kinetic energy as shown in Fig. 5.

[23]A. Zaslavsky, D. A. Grutzmacher, S. Y. Lin, T. P. Smith III, R. A. Kiehl, and T. O. Sedgwick, Phys. Rev. B **47**, 16 036 (1993).